JTTEE5 15:507-512
DOI: 10.1361/105996306X147108
1059-9630/$19.00 © ASM International

Effect of Cold Spray Deposition of a Titanium Coating on Fatigue Behavior of a Titanium Alloy

T.S. Price, P.H. Shipway, and D.G. McCartney

(Submitted February 27, 2006; in revised form May 5, 2006)

The deposition of titanium on a titanium alloy substrate is being examined for potential use as a surface treatment for medical prostheses. A Ti6Al4V alloy was coated with pure titanium by cold gas dynamic spraying. Coatings were deposited onto samples with two different surface preparation methods (as-received and grit-blasted). The fatigue life of the as-received and grit-blasted materials, both before and after coating, was measured with a rotating-bend fatigue rig. A 15% reduction in fatigue endurance limit was observed after application of the coating to the as-received substrate, but no significant reduction was observed on its application to the grit-blasted substrate. The reduction in fatigue endurance limit has been related to the substrate-coating interface properties, the elastic modulus, and the residual stress states.

Keywords CGDS, fatigue, residual stress, titanium, Ti6Al4V, Young's modulus

1. Introduction

Biomedical implants are required to not interact harmfully with the host's body, and their surface properties have been shown to significantly influence the degree of tissue interaction. A large body of research has examined chemical and morphological characteristics of biomaterial surfaces to improve biocompatibility (Ref 1-3). Pure titanium has a high level of biocompatibility, a low level of toxicity, and high resistance to corrosion by body fluids because of the presence of a very protective oxide layer. However, its fatigue and yield strength make it unsuitable for use as bulk implant material and more suitable for use as a coating. Currently many implants are produced from cobalt chrome and titanium alloys (e.g., Ti6Al4V) that are not as biocompatible as pure titanium or do not integrate as well with the bone structure (Ref 3). Hydroxyapatite (HA) coatings are used successfully, normally applied by the plasma spray process (Ref 4) to increase levels of osseointegration and patient comfort and decrease implant loosening. Comparisons between HA, grit-blasted titanium surfaces (Ref 5-8), and titanium-coated implants (Ref 9-11) have been made. Opinion is divided as to whether the effect of HA on osseointegration is either insignificant (Ref 5, 6) or positive (Ref 7-10). In studies comparing HA and titanium surfaces with identical morphologies, Hacking et al. (Ref 11) concluded that 80% of the bone appositional response was attributable to the topography of bioinert titanium. Further research in this area is required, and the search for new prosthetic surfaces is justified (Ref 11) in light of the current high levels of revision surgery.

Cold gas dynamic spraying (CGDS) involves acceleration of solid particles toward a substrate in a supersonic gas jet. Supersonic gas velocities are achieved by use of a converging-diverging de Laval nozzle (Ref 12), and particle velocities in excess of 500 m s^{-1} are generally observed at the nozzle exit. CGDS avoids high-temperature spray effects, such as vaporization, melting, and oxidation, which make it potentially attractive for application of titanium coatings. It has also been shown that titanium-HA coatings can be sprayed using the CGDS process, which may prove very desirable in terms of biocompatibility (Ref 13).

Fatigue is an important criterion to consider in the case of prosthetics because of the repeated loads exerted throughout their lifetimes. For example, a hip prosthesis may be subjected to dynamic loading of ~1-2 million load cycles per year with articulating forces reaching 3-5 times the body weight (Ref 2). The current study aims to examine the effects of CGDS-applied coatings on fatigue behavior of Ti6Al4V.

2. Experimental Methods

2.1 Materials

Commercially pure titanium (>99 wt.% Ti) feedstock powder with nominal particle size range of −45 + 5 μm was supplied by Active Metals Ltd (Sheffield, UK). Substrates for all coatings were Grade 5 Ti6Al4V. Sample surfaces were left as-received or were grit-blasted with Al_2O_3 with an average particle diameter of 250 μm. Samples of a cylindrical dog bone configuration were used for fatigue testing and produced from 7 mm diameter rod. Samples were 51 mm long and composed of shouldered ends and a central test area 19 mm in length, where the midsection was reduced to a diameter of 4 mm. The 0.2% proof and yield stresses of an as-received substrate were mea-

This article was originally published in *Building on 100 Years of Success*, *Proceedings of the 2006 International Thermal Spray Conference*, (Seattle, WA), May 15-18, 2006, B.R. Marple, M.M. Hyland, Y.-Ch. Lau, R.S. Lima, and J. Voyer, Ed., ASM International, Materials Park, 2006.

T.S. Price, P.H. Shipway, and **D.G. McCartney,** University of Nottingham, Nottingham, UK. Contact e-mail: emxtp1@nottingham.ac.uk.

sured as 880 and 800 MPa, respectively. Samples used for modulus testing measured 16 × 120 × 1.6 mm. Pull-off test samples were sprayed onto 5 mm thick substrates of 45 mm diameter.

2.2 Cold Spraying Process

CGDS at the University of Nottingham utilized a de Laval nozzle 100 mm long with an area expansion ratio of ~7.6. Room temperature helium was used as the carrier and main gas. The carrier gas pressure was maintained at 30 bar and ~1 bar above that of the main driving gas. An optimized stand-off distance of 20 mm was used. A high-pressure powder feeder (1264HP, Praxair, Rochester, MN) was used with a powder feed wheel speed of 2 rpm. All samples were degreased in alcohol immediately prior to spraying.

During spraying, fatigue samples were rotated at ~2800 rpm and traversed relative to the CGDS nozzle at 100 mm s^{-1} to achieve an even coating on the surface. Coatings, ~120 μm thick, were applied to the central 21 mm of the sample so that they covered the central test area and a small part of the shoulders. Modulus testing samples were traversed relative to the CGDS gun at 500 mm s^{-1}. The coating, ~700 μm thick, was deposited centrally onto the largest face of the test strip, covering an area measuring 80 × 16 mm. Coatings for bond-strength tests were produced using a mask to create a circular deposit 8.16 mm in diameter and ~400 μm thick.

2.3 Characterization of Coatings

Examination of fatigue samples was performed by scanning electron microscopy (SEM, XL30, Philips, Eindhoven, The Netherlands) operated at 20 kV, utilizing both secondary electron (SE) and back-scattered electron (BSE) imaging. Fatigue surfaces were examined with no modification to the surface. Sections of the coatings were taken perpendicular to the substrate-coating interface. These were mounted in a conducting resin and then ground and polished using a colloidal SiO_2 suspension in H_2O_2.

2.4 Bond-Strength Test Methodology

The bond strength of the coatings was tested by using a hydraulic adhesion/tensile equipment (PAT, DFD Instruments, Kristiansand, Norway). The circular sprayed area was glued to the test element with a heat-cured epoxy resin.

2.5 Fatigue Testing Methodology

A Wohler rotating bend fatigue testing machine was used. Samples were rotated at ~3000 rpm. A fatigue step loading method was used. This method is widely used (Ref 14-18) because it addresses the statistical problems associated with fatigue testing (Ref 16). Starting with an applied load known to not cause failure, the sample is rotated for 10^7 cycles. The load applied is then increased by steps of 5%, and the process is repeated until failure occurs (Ref 16). The data are interpolated to calculate the applied stress required for failure to occur at 10^7 cycles. This constant life endurance stress is termed the endurance limit (Ref 15). Up to five samples of each sample type were tested to allow an average fatigue endurance limit to be calculated. One potential problem of the step loading method is coaxing (Ref 15, 18), where fatigue at loads under which the sample does not fail alters its endurance limit. However, it has been shown that coaxing is not significant in Ti6Al4V (Ref 16, 18).

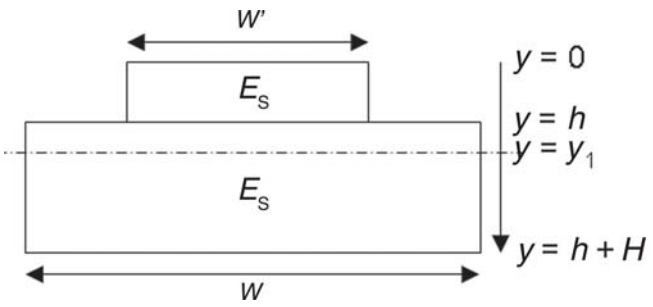

Fig. 1 Geometry of the equivalent section

2.6 Modulus Testing Methodology

Determination of the residual stress in the coating by mechanical methods requires knowledge of both the coating and substrate modulus. These moduli were determined using a four-point bend test methodology. During bend testing, samples were tested three times with the coatings in compression, from which an average elastic modulus was calculated. The midpoint displacement of the surface in tension was monitored using an external linear variable displacement transducer (LVDT, Model 1000RA, RDP Electronics Ltd, Wolverhampton, UK) to an accuracy of ±1 μm.

The modulus, E, of a uniform beam can be calculated from the slope of the load-displacement curve and is given by (Ref 19):

$$E = \frac{Pa}{24vI}(3L^2 - 4a^2) \quad \text{(Eq 1)}$$

where v is the midpoint displacement, L is the distance between outer support rollers (50 mm in this work), a is the distance between the loading and support rollers (15 mm in this work), and P is the applied load per loading point. I is the second moment of area, given by:

$$I = \frac{wd^3}{12} \quad \text{(Eq 2)}$$

where w is the width and d the depth of the sample. However, if the beam is created from two dissimilar materials (i.e., a substrate and coating), the method of equivalent sections must be used to find the location of the neutral axis (Ref 20).

2.7 Method of Equivalent Sections

This method replaces the actual section with a mechanically equivalent one, in which all the material has a common modulus. If the elastic moduli of the substrate and coating are E_s and E_c, respectively, and w is the original width of the coating, then w' is the equivalent section width of the coating with an elastic modulus E_s, as shown in Fig. 1. H and h are the substrate and coating thicknesses respectively. w' is given by:

$$w' = w\left(\frac{E_c}{E_s}\right) \quad \text{(Eq 3)}$$

The distance between the neutral axis of the composite beam and the free coating surface, y_1, is given by:

$$y_1 = \frac{h^2E_c + E_sH(H+2h)}{2(HE_s + hE_c)} \quad \text{(Eq 4)}$$

The second moment of area, I, of the composite beam can be shown to be equal to

$$I = \left[\frac{wH^3}{12} + (wH)\left(\left(h + \frac{H}{2}\right) - y_1\right)^2\right] + \left[\frac{w'h^3}{12} + (wh)\left(y_1 - \left(\frac{h}{2}\right)\right)^2\right] \quad \text{(Eq 5)}$$

For unsprayed samples, Eq 1 can be used to calculate the modulus of the substrate using the slope of the load-displacement curve generated from the four-point bend test. To calculate the elastic modulus of the coating, the coated sample is treated as a composite beam. Using Eq 1 and the slope of the load-displacement curve of the coated samples, it is possible to determine the value of the product EI of the composite beam. Using Eq 4 and 5, the known E_s values, and an estimate of E_c, an estimated EI value can be made and compared with the experimentally derived value. E_c is then refined.

2.8 Residual Stress-Deflection Method Test Methodology

Residual stresses developed during spraying were estimated from the induced bending of the sample. Prior to spraying, the underside of the substrate was profiled using a Talysurf CLI (Leicester, UK) 1000 with a stylus having a resolution of 40 nm. Profiling was carried out again after spraying to allow the radius of curvature of the beam, R, associated with the residual stresses to be measured.

The substrate and coating are considered to be a composite beam of two dissimilar materials. Due to the misfit strain between the coating and substrate, forces equal but opposite in magnitude occur. These forces act at the center of the two sections to give a continuity of length (Ref 20) as shown by Fig. 2.

The moment associated with the forces is given by:

$$M = P\left(\frac{h+H}{2}\right) \quad \text{(Eq 6)}$$

Balancing this moment will cause the beam to bend to give a radius of curvature, R. The stress, σ, in the beam is proportional to the distance, $(y_1 - y)$, from its neutral axis where E_y is the beam modulus (a function of the position; Ref 20).

$$\frac{\sigma}{(y_1 - y)} = \frac{E_y}{R} \quad \text{(Eq 7)}$$

Considering an element of cross sectional area dA at a distance $(y_1 - y)$ from the neutral axis and assuming that for pure bending

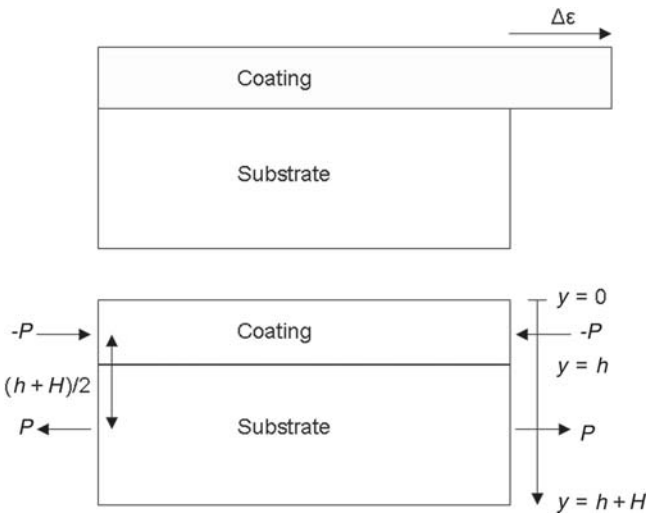

Fig. 2 Schematic of the misfit strain between the coating and the substrate

the normal net force on the cross section must be zero (Ref 20), then the bending moment is given by:

$$M = \frac{w}{R}\int_0^{h+H} E_y(y_1 - y)^2\,dy \quad \text{(Eq 8)}$$

Solving Eq 8 and inserting Eq 6 gives:

$$P\left(\frac{h+H}{2}\right) = \frac{wE_c}{R}\left(y_1^2h - h^2y_1 + \frac{h^3}{3}\right) + \frac{wE_s}{R}\left(y_1(H^2 + 2hH - Hy_1) + \frac{h^3}{3} - \frac{(h+H)^3}{3}\right) \quad \text{(Eq 9)}$$

where y_1 is given by Eq 4. Because $\varepsilon_s = \sigma/E_s$ and $\sigma = P/Hw$, and similarly for ε_c, then if $\Delta\varepsilon = \varepsilon_s - \varepsilon_c$, then (Ref 20):

$$\Delta\varepsilon = \frac{P}{HwE_s} + \frac{P}{hwE_c} \quad \text{(Eq 10)}$$

$$\therefore \frac{P}{w} = \Delta\varepsilon\left(\frac{hE_cHE_s}{hE_c + HE_s}\right) \quad \text{(Eq 11)}$$

The stress distributions within the coating and substrate can be determined by using the values of P and R from $\sigma/y = E/R$. Therefore, the stresses in the coating at the free surface ($y = 0$) and at the substrate-coating interface ($y = h$) are given by

$$\sigma_c\Big|_{y=0} = -\Delta\varepsilon\left(\frac{E_cHE_s}{hE_c + HE_s}\right) + E_c\frac{y_1}{R} \quad \text{(Eq 12)}$$

$$\sigma_c\Big|_{y=h} = -\Delta\varepsilon\left(\frac{E_cHE_s}{hE_c + HE_s}\right) + E_c\frac{(h - y_1)}{R} \quad \text{(Eq 13)}$$

Table 1 Effect of surface finish on fatigue endurance limit

Surface finish	Surface roughness, Ra, μm	Fatigue endurance limit, MPa	Modulus, GPa
As-received	~2.7	633	107
As-received and sprayed	~8.6	537	20
Grit-blasted	~3.5	507	107
Grit-blasted and sprayed	~8.5	512	19

while the stresses in the substrate at the substrate-coating interface ($y = h$) are calculated by:

$$\sigma_s\Big|_{y=h} = -\Delta\varepsilon\left(\frac{hE_cE_s}{hE_c + HE_s}\right) + E_s\frac{(h - y_1)}{R} \quad \text{(Eq 14)}$$

3. Results

3.1 Fatigue Data

Table 1 shows the endurance life of the two surface finishes of the substrate with and without a CGDS-applied coating. It can be seen that both grit blasting and the CGDS process have a significant effect on the fatigue endurance limit. The effect of applying a cold-sprayed titanium coating after grit blasting does not reduce the fatigue endurance limit further. Endurance limits and reductions caused by grit blasting reported in this paper are comparable to those reported elsewhere (Ref 14).

In general, fatigue failures tend to start at the surface of a component and surface properties that affect fatigue can be divided into three categories (Ref 14, 21): (a) surface roughness or stress raisers; (b) changes in the fatigue strength of the surface metal; and (c) changes in the residual stress at the surface. It is generally argued that smooth surfaces have a longer fatigue life as they have fewer stress raisers. Compressive residual stresses at the surface will increase fatigue life.

3.2 Bond-Strength Results

Bond-strength results for coatings applied to as-received (Ra ≈ 2.6 μm) and grit-blasted (Ra ≈ 3.5 μm) substrate finishes were 37 and 32 MPa, respectively. In a significant number of the tests, failure occurred within the resin, indicating that the coating-substrate bond strength was higher than this value. An as-received surface finish showed slightly higher bond strength than the grit-blasted samples. This could be due to the work hardening associated to the grit-blasting treatment of the substrate surface, therefore making it more difficult for the sprayed coating to bond to the substrate.

3.3 Analysis of Fracture Behavior

The as-received samples exhibited the structural features commonly observed in fatigue fractures. Examples of slip band formation, stage I and II crack growth, could be seen. The grit-blasted samples exhibited a 20% reduction in fatigue endurance limit. This is expected to be due to the grit-blasting process producing surface stress raisers. SEM showed similar fracture features to the as-received samples.

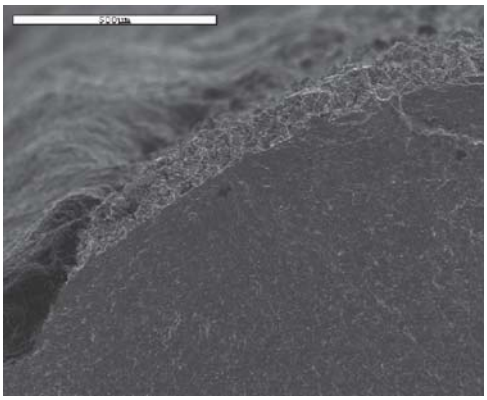

Fig. 3 SE image showing initial fracture of the as-received Ti6Al4V substrate and the Ti coating

Figure 3 shows that, in the as-received and sprayed samples, there was little deformation to the coating itself at the point of initial fracture and it appeared well bonded to the substrate. In contrast, in the regions associated with the final failure, the coating was seen to have debonded from the substrate.

Cross-sectional SE images, Fig. 4(a) and (b), show the difference in degradation of the coating at the point of fatigue fracture and close to the shoulder of the sample where a much lower level of alternating stress was experienced. Close to the fracture surface (Fig. 4a), coating delamination from the substrate can be seen along with debonding of particles within the coating itself.

In the grit-blasted and sprayed samples, coating delamination close to the initial point of fatigue fracture was observed (Fig. 5). This is in contrast to the behavior observed for the coating sprayed onto the as-received surface (Fig. 3) and may be due to more stress raisers at the substrate surface, which increase the likelihood of crack formation and coating delamination.

3.4 Modulus Testing

Modulus values for the substrate and coating are shown in Table 1 for the coating tested in compression. The modulus of the coating is shown to be ~20% of that of the substrate material.

3.5 Residual Stress Measurement

It is possible to measure by profilometry the radius of curvature of the beam samples caused by application of the coatings. From these measured values and the measured Young's moduli, the residual stresses can be calculated (Table 2). It can be seen that stresses in the coatings are small and compressive; accordingly, tensile stresses are expected in the substrate close to the interface.

4. Discussion

Application of CGDS titanium coatings has been shown to reduce the fatigue endurance limit. This is caused by modification (roughening) of the substrate surface due to impinging high-velocity particles and tensile residual stresses within the substrate at the substrate-coating interface. Surface roughening of

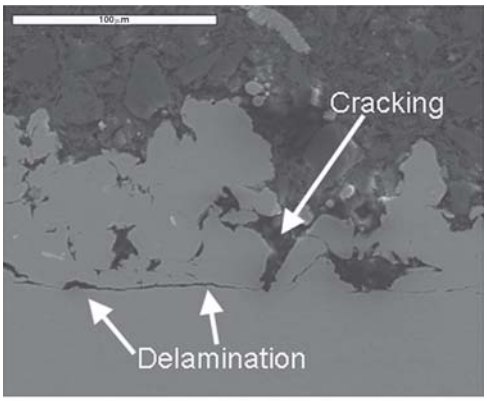

(a)

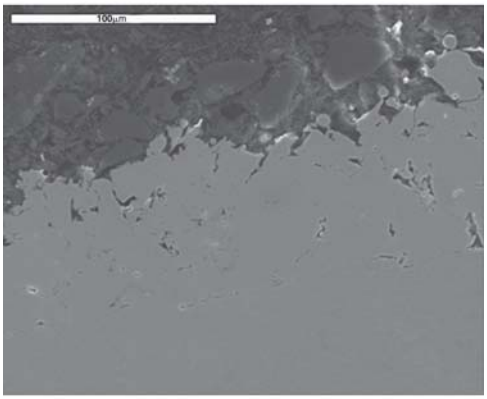

(b)

Fig. 4 SE image of the cross section of the as-received Ti6Al4V substrate and the Ti coating (a) close to the fatigue fracture (stress ≈ 570 MPa) and (b) away from the fatigue fracture (stress ≈ 190 MPa)

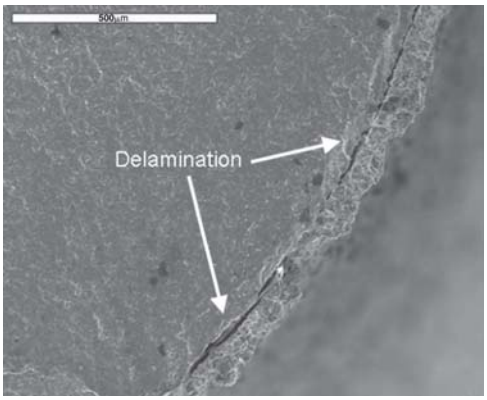

Fig. 5 SE image showing initial fracture surface of the grit-blasted Ti6Al4V substrate and the Ti coating

the substrate will increase the possible number of crack nucleation sites.

The modulus values of the titanium coating were found to be much lower than that of bulk material (~20 GPa). This result is in accord with modulus values of between 15 and 30 GPa reported for titanium coatings deposited by CGDS with heated nitrogen (Ref 22). Similarly, in plasma spraying, Kuroda and Clyne (Ref 23) show that coatings of a wide range of materials have a modulus approximately one-third that of the corresponding bulk value. The low modulus values found were attributed to the poor lateral bonding between individual splats (Ref 23). The CGDS coatings generated within this report have shown modulus values approximately one-fifth that of the bulk material, and this again indicates much of the deformation of the coating under load is taken up by movement across the particle-particle interfaces, implying that the lateral bonding between splats is not strong.

Table 2 Residual stresses within the coating and the substrate

	As-received and sprayed, MPa	Grit-blasted and sprayed, MPa
σ_c at $y = 0$	−25	−10
σ_c at $y = h$	−32	−13
σ_s at $y = h$	+52	+21

Although the residual stress estimates indicate that the stress will be tensile in the substrate close to the interface, these stresses will be reduced by the compressive stresses that will be present in this region as a result of the impact of the first depositing particles. It is unknown if the cracks initiate at the substrate-coating interface or coating-free surface and at what point the coating delaminates from the substrate. Residual stress measurements show low stresses generated within the coating and substrate due to the CGDS process. However, the method used to measure these data would have allowed stress relaxation caused by deflection in the samples. The fatigue test samples (which are axisymmetric) would have not allowed stress relaxation during spraying; therefore, stresses within these samples would be expected to be higher than those shown in Table 2. Residual stresses within the CGDS titanium coatings have been shown to be of a compressive nature. The values found are comparable to other from the literature (Ref 24) and are expected to be low due to minimization of thermal effects during cold spraying.

Figure 4(a) and (b) show the significant effect of the fatigue testing on the bonding within the coating and at the interface. Near to the fracture, areas of the coating have debonded along splat boundaries and at the substrate-coating interface. At the shoulder of the sample where applied stresses were lower, the coating shows little sign of degradation.

The fatigue endurance limit is similar for the grit-blasted and grit-blasted-and-sprayed samples. Both show a lower fatigue endurance limit than the as-received and sprayed samples. This is due to the grit blasting process deforming the substrate surface and creating a large number of stress raisers. It is notable that the addition of the coating to the as-received sample results in a reduction in fatigue endurance limit of ~96 MPa, whereas addition of the coating to the grit-blasted substrates results in a negligible change in the endurance limit. The stresses in the coatings and substrates for both substrate types are similar, differing by up to ~30 MPa (Table 2), and they do not account for this difference. It must therefore be concluded that the reduction in endurance limit for the grit-blasted substrates is dominated by the stress raisers produced during grit blasting, leaving the endurance limit relatively insensitive to any residual stresses resulting from the addition of the coating.

5. Conclusions

CGDS titanium coatings have been successfully deposited on a Ti6Al4V substrate with reasonable bond strengths. Low modulus values for the coating have been recorded that can be attributed to poor intersplat bonding. It has been shown that CGDS titanium coatings have a detrimental effect on the fatigue endurance limit of Ti6Al4V. Reasons for this are due to variation in the substrate surface topography and induced tensile residual stresses within the substrate, both caused by the CGDS process. Compressive stresses found within a coating are usually associated with increased fatigue endurance limits; however, those found within CGDS titanium coatings are too low to prevent fatigue crack formation, and these lead to premature fracture.

Acknowledgments

T.S. Price acknowledges financial support from the Nottingham Innovative Manufacturing Research Centre and the EPSRC in the form of a Ph.D. Studentship.

References

1. G. Rizzi, A. Scrivani, M. Fini, and R. Giardino, Biomedical Coatings to Improve the Tissue-Biomaterial Interface, *Int. J. Artif. Organs,* 2004, **27,** p 649-657
2. D.M. Brunette, Principles of Cell Behavior on Titanium Surfaces and Their Application to Implanted Devices, D.M. Brunette, P. Tengvall, M. Textor, and P. Thomsen, Ed., *Titanium in Medicine: Material Science, Surface Science, Engineering, Biological Responses and Medical Applications,* Springer-Verlag, 2001, p 485-512
3. J. Breme, E. Eisenbarth, and V. Biehl, Titanium and Its Alloys for Medical Applications, *Titanium and Titanium Alloys: Fundamentals and Applications,* C. Leyens and M. Peters, Ed., Wiley-VCH, 2003, p 423-452
4. J. Dumbleton and M.T. Manley, Current Concepts Review: Hydroxyapatite-Coated Prostheses in Total Hip and Knee Arthroplasty, *J. Bone Joint Surg. Am.,* 2004, **86A,** p 2526-2540
5. L. Carlsson, L. Regner, C. Johansson, M. Gottlander, and P. Herberts, Bone Response to Hydroxyapatite-Coated and Commercially Pure Titanium Implants in the Human Arthritic Knee, *J. Orthop. Res.,* 1994, **12,** p 274-285
6. A.J.M. Yee, H.K. Kreder, I. Bookman, and J.R. Davey, A Randomized Trial of Hydroxyapatite Coated Prostheses in Total Hip Arthroplasty, *Clin. Orthop.,* 1999, **366,** p 120-132
7. M. Hamadouche, J. Witvoet, R. Porcher, A. Meunier, L. Sedel, and R. Nizard, Hydroxyapatite-Coated versus Grit-Blasted Femoral Stems: A Prospective, Randomised Study Using EBRA-FCA, *J. Bone Joint Surg. Br.,* 2001, **83B,** p 979-987
8. A. Eckardt, H.M. Aberman, H.D. Cantwell, and J. Heine, Biological Fixation of Hydroxyapatite-Coated versus Grit-Blasted Titanium Hip Stems: A Canine Study, *Arch. Orthop. Trauma Surg.,* 2003, **123,** p 28-35
9. N. Aebli, J. Krebs, H. Stich, P. Schawalder, M. Walton, D. Schwenke, H. Gruner, B. Gasser, and J.C. Theis, In Vivo Comparison of the Osseointegration of Vacuum Plasma Sprayed Titanium- and Hydroxyapatite-Coated Implants, *J. Biomed. Mater. Res. Part A,* 2003, **66A,** p 356-363
10. Y.H. Kim, J.S. Kim, S.H. Oh, and J.M. Kim, Comparison of Porous-Coated Titanium Femoral Stems with and without Hydroxyapatite Coating, *J. Bone Joint Surg. Am.,* 2003, **85A,** p 1682-1688
11. S.A. Hacking, M. Tanzer, E.J. Harvey, J.J. Krygier, and J.D. Bobyn, Relative Contributions of Chemistry and Topography to the Osseointegration of Hydroxyapatite Coatings, *Clin. Orthop.,* 2002, **405,** p 24-38
12. R.C. Dykhuizen and M.F. Smith, Gas Dynamic Principles of Cold Spray, *J. Therm. Spray Technol.,* 1998, **7,** p 205-212
13. V. Shukla, G.S. Elliott, B.H. Kear, and L.E. McCandlish, Hyperkinetic Deposition of Nanopowders by Supersonic Rectangular Jet Impingement, *Scr. Mater.,* 2001, **44,** p 2179-2182
14. M. Baleani, M. Viceconti, and A. Toni, The Effect of Sandblasting Treatment on Endurance Properties of Titanium Alloy Hip Prostheses, *Artif. Organs,* 2000, **24,** p 296-299
15. R.S. Bellows, S. Muju, and T. Nicholas, Validation of the Step Test Method for Generating Haigh Diagrams for Ti-6Al-4V, *Int. J. Fatigue,* 1999, **21,** p 687-697
16. D.C. Maxwell and T. Nicholas, A Rapid Method for Generation of a Haigh Diagram for High Cycle Fatigue, ASTM STP 1332, Fatigue and Fracture Mechanics, Vol. 29, T.L. Panontin and S.D. Sheppard, Ed., ASM International 1999, p 626-641
17. S.R. Thompson, J.J. Ruschau, and T. Nicholas, Influence of Residual Stresses on High Cycle Fatigue Strength of Ti-6Al-4V Subjected to Foreign Object Damage, *Int. J. Fatigue,* 2001, **23,** p S405-S412
18. T. Nicholas, Step Loading for Very High Cycle Fatigue, *Fatigue Fract. Eng. Mater. Struct.,* 2002, **25,** p 861-869
19. E.P. Popov and T.A. Balan, *Engineering Mechanics of Solids,* 2nd ed., Prentice-Hall, Inc., 1999
20. T.W. Clyne and S.C. Gill, Residual Stresses in Thermal Spray Coatings and Their Effect on Interfacial Adhesion: A Review of Recent Work, *J. Therm. Spray Technol.,* 1996, **5,** p 401-418
21. G.E. Dieter, *Mechanical Metallurgy*, 3rd ed., McGraw-Hill, 1986
22. R.S. Lima, A. Kucuk, C.C. Berndt, J. Karthikeyan, C.M. Kay, and J. Lindemann, Deposition Efficiency, Mechanical Properties and Coating Roughness in Cold-Sprayed Titanium, *J. Mater. Sci. Lett.,* 2002, **21,** p 1687-1689
23. S. Kuroda and T.W. Clyne, The Quenching Stress in Thermally Sprayed Coatings, *Thin Solid Films,* 1991, **200,** p 49-66
24. S. Sampath, X.Y. Jiang, J. Matejicek, L. Prchlik, A. Kulkarni, and A. Vaidya, Role of Thermal Spray Processing Method on the Microstructure, Residual Stress and Properties of Coatings: An Integrated Study for Ni-5 wt.% Al Bond Coats, *Mater. Sci. Eng. A,* 2004, **364,** p 216-231